- -

Chiral Truxene-Based Self-Assembled Cages: Triple Interlocking and Supramolecular Chirogenesis

- -

Séjourné, Simon; Labrunie, Antoine; Dalinot, Clément; Canevet, David; Geuchaichia, Romain; Bou Zeid, Jennifer; Benchohra, Amina; Cauchy, Thomas; Arnaud, Brosseau; Allain, Magali; Chamignon, Cécile; Viger-Gravel, Jasmine; Pintacuda, Guido; Carré, Vincent [**and 4 more**]

This publication URL: https://archive-ouverte.unige.ch/unige:174680
Publication DOI: 10.1002/anie.202400961

Accepted Article

Authors: Simon Séjourné, Antoine Labrunie, Clément Dalinot, David Canevet, Romain Geuchaichia, Jennifer Bou Zeid, Amina Benchohra, Thomas Cauchy, Brosseau Arnaud, Magali Allain, Cécile Chamignon, Jasmine Viger-Gravel, Guido Pintacuda, Vincent Carré, Frédéric Aubriet, Nicolas Vanthuyne, Marc Sallé, and Sébastien Goeb

This manuscript has been accepted after peer review and appears as an Accepted Article online prior to editing, proofing, and formal publication of the final Version of Record (VoR). The VoR will be published online in Early View as soon as possible and may be different to this Accepted Article as a result of editing. Readers should obtain the VoR from the journal website shown below when it is published to ensure accuracy of information. The authors are responsible for the content of this Accepted Article.

WILEY VCH

RESEARCH ARTICLE

Chiral Truxene-Based Self-Assembled Cages: Triple Interlocking and Supramolecular Chirogenesis

Simon Séjourné,[a] Antoine Labrunie,[a] Clément Dalinot,[a] David Canevet,[a] Romain Guechaichia,[a] Jennifer Bou Zeid,[a] Amina Benchohra,[a] Thomas Cauchy,[a] Arnaud Brosseau,[a] Magali Allain,[a] Cécile Chamignon,[b] Jasmine Viger-Gravel,[b] Guido Pintacuda,[b] Vincent Carré,[c] Frédéric Aubriet,[c] Nicolas Vanthuyne,[d] Marc Sallé*[a] and Sébastien Goeb*[a]

[a]   Dr. S. Séjourné, Dr. A. Labrunie, Dr. C. Dalinot, Prof. D. Canevet, Mr. R. Guechaichia, Ms. J. Bou Zeid, Dr. A. Benchohra, Dr. T. Cauchy, Mr. A. Brosseau, Dr. M. Allain, Prof. M. Sallé, Dr. S. Goeb
        Univ Angers, CNRS, MOLTECH-ANJOU, F-49000 Angers, France
        E-mail: marc.salle@univ-angers.fr; sebastien.goeb@univ-angers.fr
[b]   Ms Cécile Chamignon, Dr. J. Viger-Gravel, Dr. G. Pintacuda
        Centre de RMN à Très Hauts Champs, Université de Lyon (UMR 5082 CNRS/Ecole Normale Supérieure/Université Claude Bernard Lyon 1), 69100 Villeurbanne, France
[c]   Prof. V. Carré, Prof. F. Aubriet
        Université de Lorraine, LCP-A2MC, F-57000 Metz, France
[d]   Dr. N. Vanthuyne
        Aix Marseille Université, CNRS, Centrale Marseille, iSm2, F-13397 Marseille, France

        Supporting information for this article is given via a link at the end of the document.

Abstract: Incorporating chiral elements in host-guest systems currently focuses much attention, which results from the major impact such structures may have onto a wide range of applications, from pharmaceuticals to materials science and beyond. Moreover, the development of multi-responsive and -functional systems is highly desirable since they offer numerous benefits. In this context, we describe herein the construction of a metal-driven self-assembled cage that associates a chiral truxene-based ligand and a bis-ruthenium complex. The maximum separation between both facing chiral units in the assembly is fixed by the intermetallic distance within the lateral bis-ruthenium complex (8.4 Å). The resulting chiral cavity was shown to encapsulate polyaromatic guest molecules, but also to afford a chiral triply interlocked [2]catenane structure. The formation of the latter occurs at high concentration, while its disassembly could be achieved by addition of a planar achiral molecule. Interestingly the latter exhibits induced circular dichroism signature when trapped within the chiral cavity, demonstrating the cage ability for inducing supramolecular chirogenesis.

Introduction

The coordination-driven self-assembly constitutes a versatile and fascinating approach, garnering considerable attention by the supramolecular chemists community in recent decades.[1] This unique strategy relies on the directional coordination of metal ions with organic ligands, producing in one-step intricate and well-defined architectures.

The ability to create such complex structures, which generally feature a cavity prone to accommodate various substrates, has opened up new horizons in the field of molecular recognition,[2] with diverse applications[3] in catalysis,[4] remediation,[5] drug delivery,[6] sensors,[7] for instance. By engineering ligands with specific functional groups, it is possible to design host molecules

with high affinity and selectivity for particular guests. Moreover, in some cases, the dynamic nature of these host assemblies may allow for the reversible binding and release of the guest molecule,[8] triggered by a variety of stimuli, including pH changes,[9] addition of a chemical,[10] or by photo-[11] or redox-activation.[12]

In recent years, a growing interest has emerged in the development of chiral host molecules using the coordination-driven self-assembly approach. Using chiral ligands along the synthetic process allows to reach chiral host coordination cages, whose cavities display distinct handedness. Enantioselective interactions may occur with chiral guest molecules, a situation of interest for enantioseparation, asymmetric catalysis, or chiral sensing.[13] Supramolecular chirogenesis represents an efficient way to express chirality in artificial systems,[14] and involves non-covalent chiral recognition between the host and guest species. This phenomenon, which has notably been reported for tweezers,[15] macrocycles[16] and cages[17] or miscellaneous systems,[18] arises from the asymmetric induction and amplification of chirality occurring between the host and guest, even when one or both lack inherent chirality.

We recently discussed how the achiral hexa-alkylated truxene ligand **A** can form polyhedra (M₆L₂ stoichiometry). Upon self-assembling with bis(metallic) Ruthenium or Rhodium complexes,[19] this achiral ligand proved to form cages existing as chiral face-rotating stereoisomers. By adjusting the length of the six alkyl chains and the distance between the truxene cores in those self-assembled structures (i.e. the metal-to-metal distance), we were able to control the distribution of homo- and hetero-chiral diastereoisomers. For instance, association of ligand **A** and complex **Ru** afforded only a couple of enantiomers upon chiral self-sorting (Figure 1a).[19b] Their cavity is partially obstructed by six butyl chains (three from each facing truxene platforms), which prevented any guest molecules from accessing the cavity or even cages interlocking. Inspired by these results obtained from an

RESEARCH ARTICLE

achiral ligand, we defined two new objectives: i) to construct an empty chiral cavity capable of accommodating planar achiral guests and ii) as an extension, to generate interlocked chiral dimeric cages in a control manner. The fascinating family of interlocked cages[20] is the subject of an intense current interest due to original geometric characteristics, which may unveil new category of materials with exciting properties.[21] To achieve those two objectives orienting the self-assembly process towards an empty cavity appeared necessary. In this context, we anticipated that such a condition may be reached upon self-assembling: i) a bis-Ruthenium complex (**Ru**), displaying a metal-to-metal distance of 8.4 Å,[22] and ii) a chiral *syn*-substituted truxene-based ligand (**L**) endowed with only three *n*-butyl chains (Figure 1).
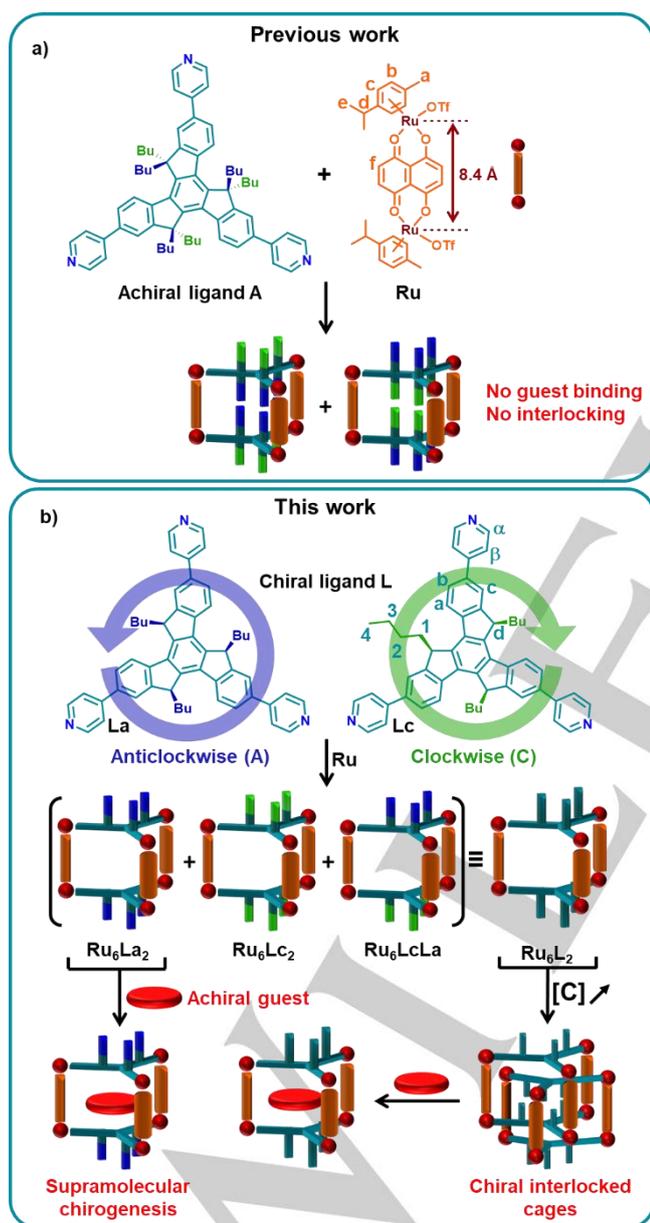
Figure 1. Illustration of a) the previously reported chiral self-sorting process occurring upon mixing achiral ligand **A** and complex **Ru**,[19b] and b) the three stereoisomers resulting from the self-assembly reaction between chiral ligand **L** and the **Ru** complex. Their ability to undergo cage interlocking and supramolecular chirogenesis is also illustrated. **La** and **Lc** correspond to the Anticlockwise and Clockwise enantiomers of chiral ligand **L**, respectively.

Results and Discussion

The chiral ligand **L** was synthesized by adapting procedures described in the literature and is obtained as a mixture of *syn*-enantiomers (See Experimental details in the SI file).[23] It exhibits two distinct faces, a non-functionalized one –allowing π-π interactions to take place upon stacking– and another one, which is threefold alkylated with *n*-butyl groups. Alkyl chains being oriented towards the reader, each enantiomeric **Lc** or **La** form is defined by the Clockwise (C) or Anticlockwise (A) spatial orientation of the methine >CHBu bridges around the C_3-symmetric truxene platform (Figure 1b).[24] Single crystals of the racemic mixture were obtained by diffusing *n*-hexane into a dichloromethane solution of **L**.[25] Both enantiomers crystallize together in the centrosymmetric trigonal space group R-3 (Figures 2 and S96). Slightly curved truxene units dimerize in the solid state with a 60° offset, which allows π-π interactions between aromatic platforms (mean planes are separated by 3.7 Å). Thereby, butyl chains are oriented towards the exterior and the three N_{pyr} atoms of each ligand fit within a circle with a radius of 9.8 Å.
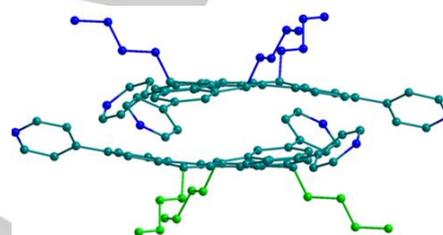

Figure 2. X-Ray crystal structures of **L** showing the presence of both enantiomers **La** and **Lc** in the crystal lattice.

Since ligand **A** generates M_6L_2 cages upon self-assembling with rigid bis metallic Ruthenium complexes,[19] we anticipated that the interaction of **L** with the complex **Ru** would produce a M_6L_2 cage (**Ru₆L₂**). In this case, it has to be noted that up to ten stereoisomers are expected, depending on the respective orientation of the butyl chains, which are either directed outward or inward relative to the cavity (Figure S1a).

The self-assembly reaction between two equivalents of **L** and three equivalents of **Ru** was carried out for 1h in methanol-d_4 (C = 10^{-3} M) at 50°C and was monitored by ^{1}H NMR spectroscopy. After one hour, the reaction reached completion, and the product could be isolated through precipitation with diethyl ether (Y = 85%). The synthesis conducted during 12h at room temperature in acetonitrile or yielded comparable outcomes.

High-resolution ESI-FTICR mass spectrometry analyses carried out in methanol or acetonitrile (Figures S78 and S79) indicated the exclusive formation of M_6L_2-type assemblies with the presence of characteristic multicharged ions [**Ru₆L₂** - 3 TfO⁻]³⁺ (m/z = 1302.5988) and [**Ru₆L₂** - 4 TfO⁻]⁴⁺ (m/z = 939.4618) or [**Ru₆L₂** - 3 TfO⁻]³⁺ (m/z = 1302.5989), [**Ru₆L₂** - 4 TfO⁻]⁴⁺ (m/z = 939.4617), and [**Ru₆L₂** - 5 TfO⁻]⁵⁺ (m/z = 721.9784) respectively. As mentioned above, a mixture of chiral species is expected from the self-assembly process. To facilitate the understanding of the corresponding NMR spectra, the subsequent nomenclature has been applied: subscripts (i and ii) are assigned to distinguish the protons of two diastereoisomers, and superscript (') is employed to represent protons located within the cavity.[26]

RESEARCH ARTICLE
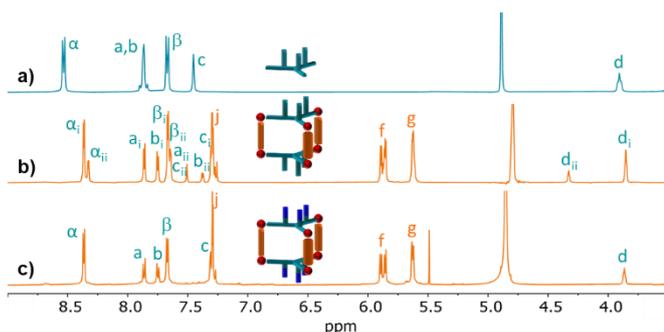
Figure 3. ^{1}H NMR spectra (298 K, C = 10^{-3} M, methanol-d[4], downfield region) of a) ligand **L**, b) cage **Ru₆L₂**, and c) cage **Ru₆La₂.** See figure 1 for ^{1}H NMR assignments.

The presence of single discrete species in solution was confirmed by ^{1}H and Diffusion-Ordered Spectroscopy (DOSY) NMR analyses, both in methanol-d[4] and acetonitrile-d[3] (Figures 3b, S12-S18). According to the Stokes-Einstein equation, the extracted diffusion coefficient D values of 3.0×10^{-10} m².s⁻¹ (methanol-d[4]) and 5.1×10^{-10} m².s⁻¹ (acetonitrile-d[3]) correspond to a hydrodynamic radius of ca. 13 Å in both cases, in accordance with a M_6L_2 stoichiometry.[27] In the case of cages built from **A**, we previously observed (Figure 1a) that the terminal methyl groups exhibit two different chemical shifts depending on their location, inside or outside the cavity (δ = -0.2 ppm and +0.35 ppm in methanol-d[4], respectively). Therefore, the observed value for protons 4 (see Figure 1b for assignments) (δ = 0.25 ppm (Figure S12)) indicates that all the butyl chains are oriented outside the cavity, limiting the number of possible stereoisomers of this M_6L_2 assembly to only three out of the 10 possible (Figures S1a (middle line) and 1b). This result is supported by the fact that all signals exhibit only one splitting pattern (Figures 3b and S12), which rules out the formation of a complex mixture of stereoisomers. Specifically, the large splitting observed for proton d, with d[i] and d[ii] at ca. 3.9 ppm and 4.3 ppm respectively, indicates the presence of a stereoisomeric mixture (i.e. one couple of enantiomers (**Ru₆Lc₂/Ru₆La₂**) and one meso form (**Ru₆LcLa**) (Figure 1b). Assigning the signals to each stereoisomer was made possible after chromatographic separation of the racemic mixture of ligand **L** (see supplementary information for details). Ligands **Lc** and **La** were then independently used to perform the same self-assembly reaction with **Ru**. By comparing the NMR spectra, the distinctive spectral patterns of the diastereoisomers were identified (Figures 3b-c, S24 and S25). Importantly, while a statistical distribution would afford a 50:50 mixture, a ratio of 75:25 was calculated upon signals integration, indicating a preference for the formation of the enantiomeric pair **Ru₆Lc₂/Ru₆La₂** over the meso **Ru₆LcLa** derivative. This chiral discrimination is attributed to the differences in π-π interactions occurring between the two facing truxene motifs within the enantiomeric pair in one hand and the meso form on the other hand. In order to gain deeper insights into the dynamics of these systems, the evolution of a mixture of the isolated **Ru₆Lc₂** and **Ru₆La₂** cages was monitored by ^{1}H NMR spectroscopy (Figure S26). No change was observed at room temperature, but an evolution of the system occurred upon heating at 50°C. After 12 hours at this temperature, the thermodynamic equilibrium was attained, and the composition of the mixture closely resembles that observed upon the self-assembly process led from racemic ligand **L**. This experiment
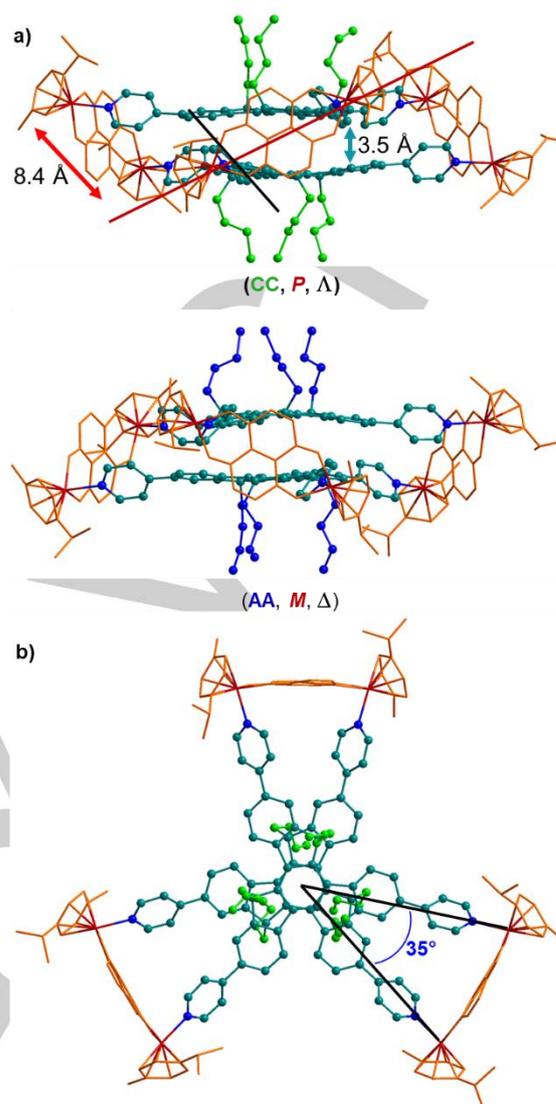

Figure 4. X-Ray crystal structures of **Ru₆L₂.**a) Lateral view showing both enantiomers **Ru₆Lc₂** and **Ru₆La₂** and b) top view of **Ru₆Lc₂.**

further confirms that the formation of these systems is thermodynamically controlled.

Single crystals of **Ru₆L₂** were obtained by vapor diffusion of MeOtBu in a methanol solution of the cage. The self-assembled structure crystallizes in the centrosymmetric space group R-3 and exhibits a large unit cell volume of ca 30,000 Å³.[26] X-ray diffraction analysis (Figures 4a and S96-S99) revealed the presence of the **Ru₆Lc₂** and **Ru₆La₂** enantiomeric pair in the crystal and confirmed that all the butyl chains are oriented outward the cavity. The interatomic distance between the two ruthenium atoms is 8.4 Å, while a notably shorter minimum distance of 3.5 Å is found between the truxene moieties. This observation definitely confirms the occurrence of π-π interactions operating between these motifs, leading to a collapse of the cage structure. This distortion is associated with a 64° tilt of the **Ru** bimetallic complexes with respect to the truxene mean planes. Consequently, the trigonal prisms are deformed, with an average Bailar angle of 35° (Figures 4b and S98).[28] Together, these

3

RESEARCH ARTICLE
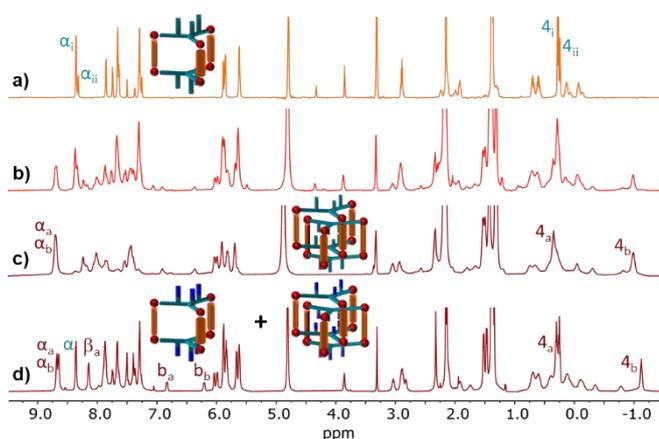
Figure 5. ^{1}H NMR spectra (298 K, methanol-d_4) resulting from the self-assembly of 2 equiv. of ligand **L** and 3 equiv. of complex **Ru** performed at a) C = 10^{-3} M, b) 10^{-2} M, c) 5×10^{-2} M and d) 2 equiv. of ligand **La** and 3 equiv. of complex **Ru** performed at 5×10^{-2} M. See figure 1 for ^{1}H NMR assignments.

parameters generate a double rosette (M/P) and a helical (Δ/Λ) chirality. Both are linked in the crystal to the configuration of the truxene ligand, since only the enantiomers (AA, M, Δ) and (CC, P, Λ) are observed.[29] While several synthetic methodologies affording macrocycles and cages have been described, the rational preparation of interlocked architectures remains a challenge due to the reduction, along the reaction, of the number of independent species, which is unfavorable in terms of entropy.[20b] Several factors can aid in achieving the locking process by providing additional driving forces to overcome this entropic cost. Such factors include π-π stacking, electrostatic interactions, hydrogen bonding, an also solvophobic effects.[20a, b, 30] These can be favored by adjusting the solvent composition, the concentration, or the temperature. On this basis and with the aim of achieving metalla-assembled interlocked cages bearing chiral units, i.e. a class of superstructures still sparsely described to date, we carried out self-assembly reactions between **L** and **Ru** at concentrations up to C = 5×10^{-2} M in methanol (C corresponds to the total concentration of cage, Figures 5 and S27). Increasing the total concentration results in significant variations in the ^{1}H NMR spectrum, as expected for an interlocked species compared to the single cage **Ru₆L₂**. The conversion appears complete from 5×10^{-2} M, as all the signals corresponding to the initially formed **Ru₆L₂** disappeared. ^{1}H DOSY NMR measurements conducted at this concentration confirm the formation of a single and larger species, with a decrease in the diffusion coefficient from D = 3.0 ×10^{-10} m².s⁻¹ (**Ru₆L₂**) to D = 1.9×10^{-10} m².s⁻¹ for the new species dimeric cage **(Ru₆L₂)₂** (Figures S32 and S33). The ^{1}H NMR spectrum of the latter species reveals a substantial shielding effect on the b aromatic signals of the truxene core, which is assigned to the emergence of novel π-π interactions between truxene ligands. Intriguingly, all signals exhibit broadening, which suggests the presence of multiple isomers in the solution. Additionally, two sets of signals for the terminal methyl groups are observed at 0.3 ppm and -1.0 ppm. The first value is comparable to that of the **Ru₆L₂** monomer cage, while the second one corresponds to the anticipated value for butyl chains situated within the cavity. This outcome suggests that certain butyl chains are oriented inside the cavity while others remain outside. The

solid obtained after addition of diethyl ether to a concentrated methanolic solution of **Ru₆L₂** at 5×10^{-2} M was analyzed using high-resolution ESI-FTICR mass spectrometry in methanol at C = 10^{-4} M (Figure S80). This measurement confirmed the formation of a $M_{12}L_4$-type species, with the presence of ions at [$Ru_{12}L_4$ - 4TfO⁻]⁴⁺ (m/z = 2028.3764), [$Ru_{12}L_4$ - 5TfO⁻]⁵⁺ (m/z = 1592.7096), and [$Ru_{12}L_4$ - 6TfO⁻]⁶⁺ (m/z = 1302.5993). Such stoichiometry is consistent with the formation of the **(Ru₆L₂)₂** species composed of two interlocked cages.

Single crystals of **(Ru₆L₂)₂** obtained by vapor diffusion of MeO*t*Bu into a concentrated solution of interlocked cages in methanol. The system crystallizes in the centrosymmetric space group C2/c with a unit cell volume of 49,000 Å³. X-ray diffraction analysis revealed the formation of an interlocked framework secured by three mechanical bonds, forming therefore a triply interlocked S_6 symmetric system composed of two cages with D_3 symmetry (Figure 6, S100 and S101).[26] Each interlocked dimer cage consists of one CC cage and one AA cage, thus forming the interlocked meso species ACAC. Contrary to the simple monomer cage **Ru₆L₂,** which displays butyl chains pointing into opposite directions, i.e. outward from the cavity, the six (2 × 3) butyl chains of a given cage point in the same direction in the interlocked dimer **(Ru₆L₂)₂**. Such arrangement is therefore consistent with the above-mentioned NMR studies, which evidenced two distinct environments for butyl chains and a strong interaction between the aromatic truxene cores. In addition, the truxene ligands appear significantly curved in **(Ru₆L₂)₂** compared to **Ru₆L₂**.
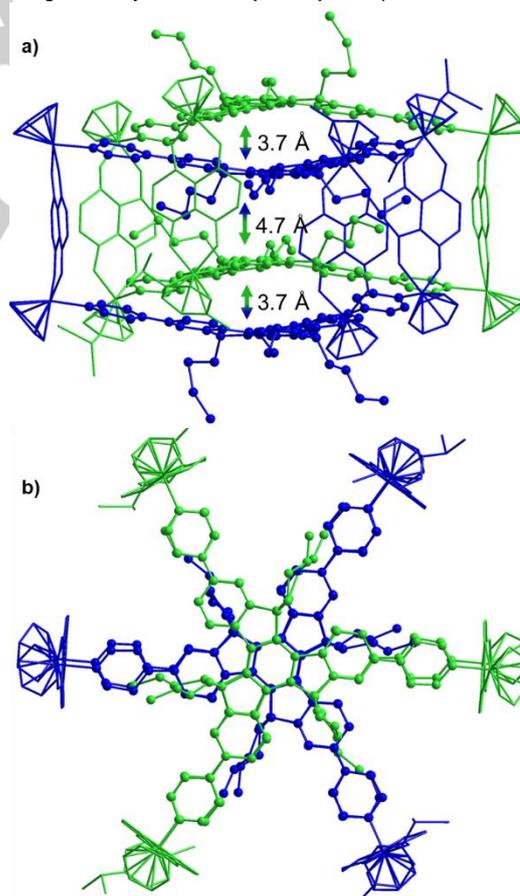

Figure 6. X-Ray crystal structures of **(Ru₆L₂)₂** (isomer ACAC), a) side view, b) top view. To facilitate comprehension, cages are represented in different colors, each corresponding to the rotation of the faces of the truxene units (see Figure 1).

4

RESEARCH ARTICLE

The successive distances between the truxene units along the stacking axis are 3.7 Å - 4.7 Å - 3.7 Å, illustrating the interaction occurring between aromatic systems when no alkyl chain is intercalated. Interestingly, the stacking mode within both truxene dimers in $(Ru_6L_2)_2$ is similar to that observed in the X-Ray structure of free ligand **L**, which spontaneously forms a dimer in the solid state with a distance of 3.7 Å (Figures 2 and S96). Finally, it is worth noting that due to the interlocking process, the bis(ruthenium) spacers of a given cage are no longer twisted, displaying a Bailar angle close to 0° (Figure 6b). X-ray diffraction measurements were performed on several sets of crystals obtained from different crystallization experiments. All of them led to the interlocked dimer $(Ru_6L_2)_2$ described above, made from one AA cage and one CC cage. This arrangement is likely preferred in order to i) minimize the steric constraints around the butyl chains and ii) favor π-π interactions between truxene platforms.

Similar experiments were conducted from the enantiopure ligand L_a. The ^{1}H NMR spectrum of a mixture of L_a and **Ru** in methanol-d_4 at 5×10^{-2} M shows, as for the racemic ligand **L**, the formation of the interlocked cages $(Ru_6La_2)_2$. Nevertheless, it is worth noting that in this case, signals corresponding to the monomer cage Ru_6La_2 still remain at this concentration (Figures 5d and S35-40). The simultaneous presence of monomeric and dimeric cages is confirmed by ^{1}H DOSY NMR, which exhibits two sets of signals at D = 2.6×10^{-10} and D = 1.9×10^{-10} m².s⁻¹ (Figure S39). These values are similar to those observed for Ru_6L_2 and $(Ru_6L_2)_2$ (Figure S33). This observation suggests a preference for the formation of the ACAC meso diastereomer over the pair of the AAAA and CCCC enantiomers. Importantly, contrary to $(Ru_6L_2)_2$, the interlocked structure $(Ru_6La_2)_2$ prepared from the enantiopure ligand **La** (AAAA arrangement) does not exhibit any signal splitting, which is particularly noticeable for the β_a, b_a, and b_b protons (Figures 5d and S35). This suggests that the racemic ligand **L** likely leads to the formation of the three stereoisomers AAAA, CCCC and ACAC. However, the presence of the other stereoisomers in solution cannot be completely ruled out (Figure S1b). By comparing the chemical shifts of the racemic and the enantiopure versions, particularly those of β_a and b_a protons (Figure S41), it appears that the prevailing form in $(Ru_6L_2)_2$ is ACAC, which is also the one characterized in the crystal structure. The three cavities comprised within the interlocked cages $(Ru_6L_2)_2$ appear too small to bind any guest molecules. In contrast, thanks to the possible tilting of the three bis(ruthenium) pillars in Ru_6L_2, the two facing truxene units which are in strong interaction when the cage in empty (Figure 4a), can be spread in order to accommodate a guest (Figure S1c). To investigate the ability of Ru_6L_2 to bind planar substrates, we conducted ^{1}H NMR experiments in acetonitrile-d_3 at a concentration of C = 10^{-3} M.[31] Various polyaromatic substrates, including coronene and **PDI-1**, were studied. The first one presents a large aromatic surface that is likely to promote interactions with the truxene core. The second one was selected for its absorption properties, notably due to the presence of signatures in the visible range outside the absorption window of the cages under consideration (see chiroptical studies). For consistency, all spectra were recorded after 2 hours at 50°C in the presence of one equivalent of the guest molecule. In both cases, important variations of chemical shifts were observed for both the substrates and the cage Ru_6L_2 (Figure 7). Considering the case of coronene as a representative example (for **PDI-1** see Figures S63-76), particularly noteworthy is the shielding of the aromatic coronene singlet and of the a and d signals of the

truxene core (Figures 7 and S47-53). This suggests an intercalation of the polyaromatic substrate in a sandwich mode between both truxene units of Ru_6L_2. This was confirmed by ^{1}H DOSY NMR spectroscopy, which shows a decrease in the diffusion coefficient assigned to coronene, from 21.0×10^{-10} m².s⁻¹ to 5.8×10^{-10} m².s⁻¹ (Figures S52 and S53) High resolution ESI-FTICR mass spectrometry measurement on a 1:1 mixture of the Ru_6L_2 cage and coronene revealed the presence of multicharged ions $[Ru_6L_2 + Coronene - 4OTf]^{4+}$ (m/z = 1014.7357) and $[Ru_6L_2 + Coronene - 5OTf]^{5+}$ (m/z = 781.9975), values which are consistent with a 1:1 stoichiometry of the host-guest complex (Figure S81). This was further confirmed by a Job plot analysis carried out by UV-visible absorption spectroscopy in acetonitrile/dichloromethane (1/1 *v/v*), a mixture of solvents chosen to ensure a good solubility of all species (Figure S77a). Finally, the host-guest association constant was determined through UV-visible titration in the same solvent mixture, highlighting a strong affinity between both components, with an association constant $K_a = 3.9 \times 10^6$ (Figure 77b). Encapsulation studies carried out with the enantiopure cage Ru_6La_2 show similar results to Ru_6L_2 (Figures S57-59), indicating equivalent complexation properties for all the diastereoisomers.

To get better insights over the guest binding mode, numerous crystallizations have been conducted on mixtures of cages and guests. Single crystals were obtained from a mixture of enantiopure Ru_6Lc_2 and **PDI-1** (Figure 8 and S102).[26] The intercalation of **PDI-1** within the cavity of Ru_6L_2 needs a significant expansion of the space between both truxene moieties, which can be attained thanks to the tilting around the bis(ruthenium) linkers (Figure S103). On this basis, the inter-truxene distance increases from 3.5 Å (Ru_6L_2) to 6.9 Å in the $PDI-1 \subset Ru_6Lc_2$ complex while the Bailar angle decreases from 35° to 23° respectively (Figure 8c).

Considering the similarity between the cavity of Ru_6L_2 when encapsulating a planar guest, and the one of the interlocked dimer $(Ru_6L_2)_2$, we decided to investigate the interconversion process between these two species. Diluting a concentrated solution in methanol-d_4 of $(Ru_6L_2)_2$ down to C = 10^{-3} M did not result in any
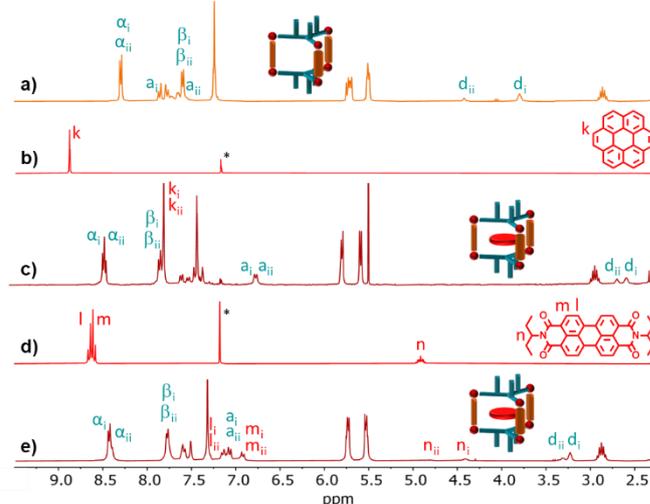
Figure 7. ^{1}H NMR spectra (298 K) of a) cage Ru_6L_2 at C = 10^{-3} M in acetonitrile-d_3, b) coronene in chloroform-d, c) cage Ru_6L_2 at C = 10^{-3} M in acetonitrile-d_3 in the presence of 1 equiv. of coronene, d) compound **PDI-1** in chloroform-d, e) cage Ru_6L_2 at C = 10^{-3} M in acetonitrile-d_3 in presence of 1 equiv. of **PDI-1**. (*) signals corresponding to residual CHCl₃ in deuterated solution. See figure 1 for ^{1}H NMR assignments.

5

RESEARCH ARTICLE

change of the NMR signals, even after refluxing solutions for several days in acetonitrile or methanol. It is worth noting that a catenane constructed from the same bis(ruthenium) complex engaged in a similar concentration-dependent experiment in our laboratory exhibits a perfect reversibility with the corresponding macrocycle in methanol-d_4.[32] This observation illustrates the high stability provided by the π-π interactions that take place between truxene units upon interlocking. The dissociation study of **(Ru₆L₂)₂** at C = 5×10^{-2} M in deuterated methanol was further conducted by adding one equivalent of coronene per cage unit and heating of the mixture at 50°C overnight. As a result, a significant simplification of the ^{1}H NMR spectrum is observed, with the complete disappearance of the signals assigned to the interlocked system (Figures 9 and S60-62). The DOSY NMR study reveals the formation of a single discrete species in solution (Figure S61) with a diffusion coefficient (D) of 2.8×10^{-10} m².s⁻¹. In comparison to **(Ru₆L₂)₂**, this value appears significantly higher and evidences the size decrease of the resulting structure. Importantly, this NMR spectrum is identical to the one recorded for the host-guest complex coronene⊂**Ru₆L₂** in the same conditions (Figure 9c), which unambiguously demonstrates the dissociation of (**Ru₆L₂)₂** upon addition of coronene, into two coronene⊂**Ru₆L₂** host-guest complexes.
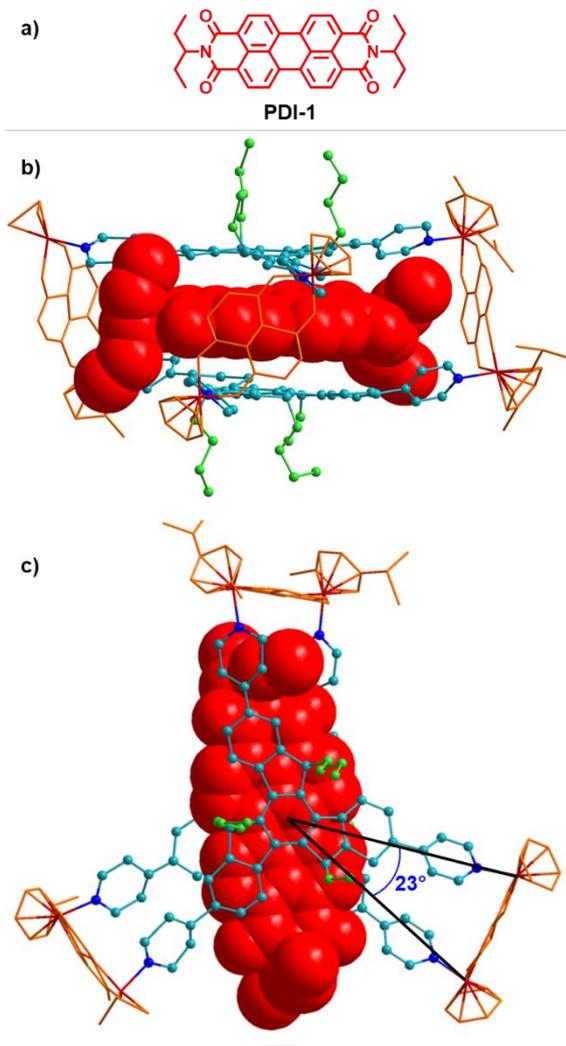
Figure 8. Representation of a) **PDI-1** and X-ray crystal structures of **PDI-1**⊂**Ru₆Lc₂**, b) side view, c) top view (with the corresponding Bailar angle).
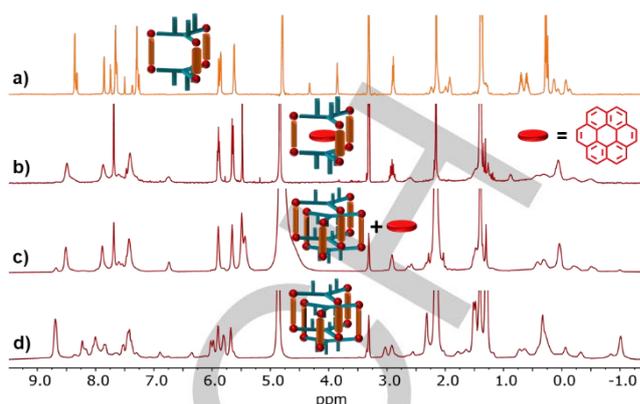
**Figure 9.** ^{1}H NMR spectra (298 K, methanol-d_4) of a) cage **Ru₆L₂** at C = 10^{-3} M, b) cage **Ru₆L₂** at C = 10^{-3} M in the presence of coronene (1 equiv.), c) interlocked cages **(Ru₆L₂)₂** at C = 5×10^{-2} M in the presence of coronene (1 equiv.) per cage and d) interlocked cages **(Ru₆L₂)₂** at C = 5×10^{-2} M.

As mentioned in the introduction, chirogenesis currently focuses much attention and notably, to design original supramolecular systems endowed with chiroptical properties. In this regard, the guest encapsulation process was followed by UV-visible absorption and circular dichroism (CD) spectroscopies. At first, the optical properties of ligand **L,** complex **Ru** and cage **Ru₆L₂** in methanol (C = 10^{-5} M) were investigated (Figure S89a and S89b). The UV-visible absorption spectrum of the cage displays similar characteristics tothe ligand ones and the metal complex when measured separately. It features an intense charge transfer band at 350 nm, with a molar absorption coefficient twice that of the ligand and exhibits a bathochromic shift due to the coordination of pyridyl rings to the metal centers. Transitions at lower energies are observed beyond 400 nm and are attributed to MLCT-type transitions.[33]

To determine the configurations of the enantiopure ligands and cages, the ground state geometries of ligand **Lc** and **La** were first optimized through Time Dependent Density Functional Theory (PBE0 functional, Figures S83 and 84), and the corresponding absorption and circular dichroism (CD) spectra were simulated (Figure S85). The latter show a good matching with experimental ones, which allowed for a straightforward identification of each enantiomer (Figure S88). The CD spectra of **Lc** and **La** display two bands in the UV region at 280 nm and 325 nm, while a large Cotton effect is observed for cages **Ru₆Lc₂** and **Ru₆La₂** above 325 nm (Figures S88 and S90).

To explore the supramolecular chirogenic properties of enantiopure cages **Ru₆Lc₂** and **Ru₆La₂**, UV-visible and circular dichroism spectroscopy measurements were additionally carried out on 1/1 mixtures of cages and **PDI-1** in methanol. As previously noted, **PDI-1** was selected for its well-adapted structural characteristics to be bound by the investigated cages, as well as for its specific absorption properties. Indeed, the chromophore exhibits an intense transition centered at 500 nm, a region at which the cages demonstrate a relatively low molar absorption coefficient. The UV-visible absorption spectra of the mixture exhibit slight variations compared to the individual components, with the only noticeable change being a red-shift in the PDI signals (Figure 10a).

6

RESEARCH ARTICLE
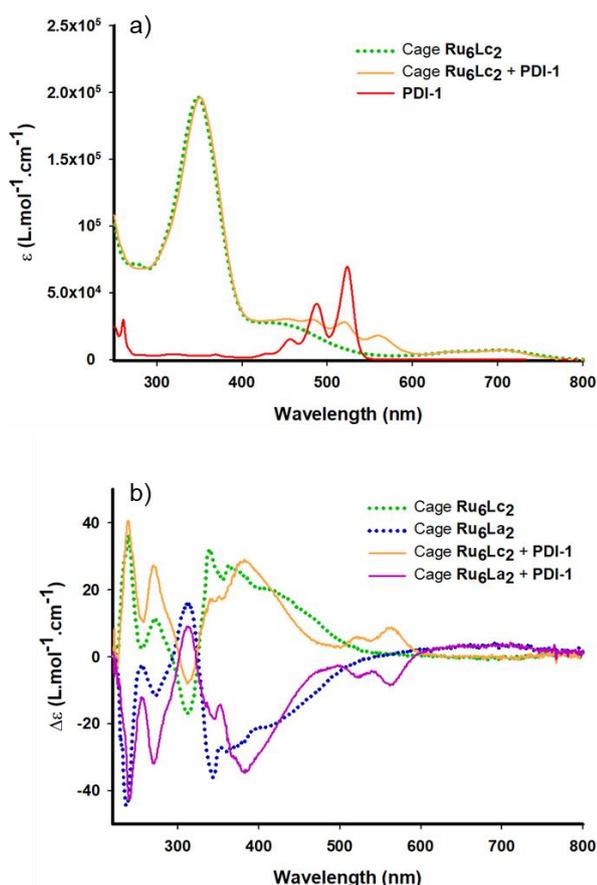
Figure 10. a) UV-vis absorption spectra of cage **Ru₆Lc₂**, a stoichiometric mixture of cage **Ru₆Lc₂** and **PDI-1**, **PDI-1**, and b) UV-visible circular dichroism spectra of cages **Ru₆Lc₂** and **Ru₆La₂**, and stoichiometric mixtures of cage **Ru₆Lc₂** and **PDI-1**, and cage **Ru₆La₂** and **PDI-1**, in methanol at C = 10⁻⁵ M.

In the presence of **PDI-1**, the circular dichroism response in the 300 nm - 480 nm region corresponding to transitions centered on the cage, is quite similar to that of the cage alone, suggesting that the structural change associated with the guest encapsulation has a moderate impact on the cage spectral signature (Figure 10b). Importantly, supramolecular chirogenesis is conclusively demonstrated by the presence of a Cotton effect between 500 nm and 600 nm with $\Delta\varepsilon = |8.4|$ cm⁻¹ M⁻¹ at C = 10⁻⁵ M, exhibiting the characteristic shape of the achiral PDI motif. The **Ru₆Lc₂** and **Ru₆La₂** host cages, with their specific three-dimensional chiral architecture derived from the face-rotating truxene components, induce chirality in the guest molecule within their cavities. The host-guest interaction creates a chiral environment that imparts a unique spatial orientation to the guest **PDI-1** molecule, thereby influencing its optical properties.

Conclusion

In summary, self-assembled cages were designed from a face-rotating truxene-based chiral ligand and a bis(ruthenium) bridging complex. Both racemic and enantiopure versions were described. The geometry provided by the complex allows the separation of

both facing ligands so as to generate a chiral cavity, well-adapted for guest recognition and cage interlocking. Interestingly, the latter chiral interpenetrated arrangement can be dissociated in the presence of a planar guest, leading to a 1:1 host guest complex. All those structures could be characterized in solution and in the solid state, including the **PDI-1⊂Ru₆Lc₂** complex. Finally, supramolecular chirogenesis could be observed in the case of the latter host-guest complex and was characterized by a circular dichroism signature of the achiral PDI guest located within the chiral environment offered by the cage. This observation was made possible thanks to strong π-stacking interactions occurring between the PDI derivative and the enantiopure chiral **Ru₆Lc₂** (and **Ru₆La₂**) cages. Work is underway to extend this approach to new families of face-rotating polyhedra, including redox-active ones.

[1]   a) A. J. McConnell, *Chem. Soc. Rev.* **2022**, *51*, 2957–2971; b) T. Tateishi, M. Yoshimura, S. Tokuda, F. Matsuda, D. Fujita, S. Furukawa, *Coord. Chem. Rev.* **2022**, *467*, 214612; c) A. E. Martin Diaz, J. E. M. Lewis, *Front. Chem.* **2021**, *9*, 706462; d) M. Hardy, A. Lützen, *Chem. Eur. J.* **2020**, *26*, 13332–13346; e) E. G. Percástegui, T. K. Ronson, J. R. Nitschke, *Chem. Rev.* **2020**, *120*, 13480–13544; f) Y. Sun, C. Chen, J. Liu, P. J. Stang, *Chem. Soc. Rev.* **2020**, *49*, 3889–3919; g) B. Li, T. He, Y. Fan, X. Yuan, H. Qiu, S. Yin, *Chem. Commun.* **2019**, *55*, 8036–8059; h) T. R. Cook, P. J. Stang, *Chem. Rev.* **2015**, *115*, 7001–7045.
[2]   a) J. E. M. Lewis, *Chem. Commun.* **2022**, *58*, 13873–13886; b) F. J. Rizzuto, L. K. S. von Krbek, J. R. Nitschke, *Nat. Rev. Chem.* **2019**, *3*, 204–222; c) C. García-Simón, M. Costas, X. Ribas, *Chem. Soc. Rev.* **2015**, *45*, 40–62; d) S. Zarra, D. M. Wood, D. A. Roberts, J. R. Nitschke, *Chem. Soc. Rev.* **2015**, *44*, 419–432.
[3]   a) S. Yadav, P. Kannan, G. Qiu, *Org. Chem. Front.* **2020**, *7*, 2842–2872; b) Y.-Y. Zhang, W.-X. Gao, L. Lin, G.-X. Jin, *Coord. Chem. Rev.* **2017**, *344*, 323–344.
[4]   a) R. Banerjee, D. Chakraborty, P. S. Mukherjee, *J. Am. Chem. Soc.* **2023**, *145*, 7692–7711; b) S. Chen, L.-J. Chen, *Chemistry* **2022**, *4*, 494–519; c) R. Saha, B. Mondal, P. S. Mukherjee, *Chem. Rev.* **2022**, *122*, 12244–12307; d) A. B. Grommet, M. Feller, R. Klajn, *Nat. Nanotechnol.* **2020**, *15*, 256–271; e) Y. Fang, J. A. Powell, E. Li, Q. Wang, Z. Perry, A. Kirchon, X. Yang, Z. Xiao, C. Zhu, L. Zhang, F. Huang, H.-C. Zhou, *Chem. Soc. Rev.* **2019**, *48*, 4707–4730; f) W.-X. Gao, H.-N. Zhang, G.-X. Jin, *Coord. Chem. Rev.* **2019**, *386*, 69–84; g) L. Zhao, X. Jing, X. Li, X.

7

Guo, L. Zeng, C. He, C. Duan, *Coord. Chem. Rev.* **2019**, *378*, 151–187; h) C. J. Brown, F. D. Toste, R. G. Bergman, K. N. Raymond, *Chem. Rev.* **2015**, *115*, 3012–3035.

[5]   E. G. Percástegui, *Chem. Commun.* **2022**, *58*, 5055–5071.

[6]   S. K. Samanta, L. Isaacs, *Coord. Chem. Rev.* **2020**, *410*, 213181.

[7]   A. Brzechwa-Chodzyńska, W. Drożdż, J. Harrowfield, A. R. Stefankiewicz, *Coord. Chem. Rev.* **2021**, *434*, 213820.

[8]   T. Y. Kim, R. A. S. Vasdev, D. Preston, J. D. Crowley, *Chem. Eur. J.* **2018**, *24*, 14878–14890.

[9]   a) I. A. Riddell, M. M. J. Smulders, J. K. Clegg, J. R. Nitschke, *Chem. Commun.* **2011**, *47*, 457–459; b) A. K.-W. Chan, W. H. Lam, Y. Tanaka, K. M.-C. Wong, V. W.-W. Yam, *Proc. Natl. Acad. Sci. USA* **2015**, *112*, 690–695.

[10]   a) Q. Gan, T. K. Ronson, D. A. Vosburg, J. D. Thoburn, J. R. Nitschke, *J. Am. Chem. Soc.* **2015**, *137*, 1770–1773; b) D. Preston, A. Fox-Charles, W. K. C. Lo, J. D. Crowley, *Chem. Commun.* **2015**, *51*, 9042–9045; c) C. S. Wood, C. Browne, D. M. Wood, J. R. Nitschke, *ACS Cent. Sci.* **2015**, *1*, 504–509; d) N. Kishi, M. Akita, M. Yoshizawa, *Angew. Chem. Int. Ed.* **2014**, *53*, 3604–3607; e) J. E. M. Lewis, E. L. Gavey, S. A. Cameron, J. D. Crowley, *Chem. Sci.* **2012**, *3*, 778–784.

[11]   a) S. M. Jansze, G. Cecot, K. Severin, *Chem. Sci.* **2018**, *9*, 4253–4257; b) M. Han, R. Michel, B. He, Y. S. Chen, D. Stalke, M. John, G. H. Clever, *Angew. Chem. Int. Ed.* **2013**, *52*, 1319–1323; c) N. Kishi, M. Akita, M. Kamiya, S. Hayashi, H.-F. Hsu, M. Yoshizawa, *J. Am. Chem. Soc.* **2013**, *135*, 12976-12979; d) T. Murase, S. Sato, M. Fujita, *Angew. Chem. Int. Ed.* **2007**, *46*, 5133–5136.

[12]   S. Goeb, M. Sallé, *Acc. Chem. Res.* **2021**, *54*, 1043–1055.

[13]   a) L. Zhang, H. Liu, G. Yuan, Y.-F. Han, *Chin. J. Chem .* **2021**, *39*, 2273–2286; b) X. Li, J. Wu, C. He, Q. Meng, C. Duan, *Small* **2019**, *15*, e1804770; c) M. Pan, K. Wu, J.-H. Zhang, C.-Y. Su, *Coord. Chem. Rev.* **2019**, *378*, 333–349; d) C. Tan, D. Chu, X. Tang, Y. Liu, W. Xuan, Y. Cui, *Chem. Eur. J.* **2019**, *25*, 662–672; e) L.-J. Chen, H.-B. Yang, M. Shionoya, *Chem. Soc. Rev.* **2017**, *46*, 2555–2576.

[14]   a) K. Kanagaraj, C. Yang, V. Borovkov in *Chirogenesis in Supramolecular Systems*, World Scientific Publishing Compagny, **2021**, pp. 85–147; b) Y. Sun, R. Aav, A. Tsuda, H. Miyake, H. Hirose, V. Borovkov, *Front. Chem.* **2021**, *9*, 679332; c) M. V. Escárcega-Bobadilla, A. W. Kleij, *Chem. Sci.* **2012**, *3*, 2421–2428.

[15]   a) J. Ren, S. Jiang, T. Han, S. Wu, Y. Tian, F. Wang, *Chem. Commun.* **2023**, *59*, 744–747; b) M. Liu, Y. Han, H. Zhong, X. Zhang, F. Wang, *Angew. Chem. Int. Ed.* **2021**, *60*, 3498–3503.

[16]   a) C. Yan, Q. Li, X. Miao, Y. Zhao, Y. Li, P. Wang, K. Wang, H. Duan, L. Zhang, L. Cao, *Angew. Chem. Int. Ed.* **2023**, *62*, e202308029; b) C. Tu, W. Wu, W. Liang, D. Zhang, W. Xu, S. Wan, W. Lu, C. Yang, *Angew. Chem. Int. Ed.* **2022**, *61*, e202203541; c) H. Zhang, L. Cheng, H. Nian, J. Du, T. Chen, L. Cao, *Chem. Commun.* **2021**, *57*, 3135–3138; d) H. Liang, B. Hua, F. Xu, L.-S. Gan, L. Shao, F. Huang, *J. Am. Chem. Soc.* **2020**, *142*, 19772-19778; e) H. Zhu, Q. Li, Z. Gao, H. Wang, B. Shi, Y. Wu, L. Shangguan, X. Hong, F. Wang, F. Huang, *Angew. Chem. Int. Ed.* **2020**, *59*, 10868–10872; f) L.-L. Wang, Z. Chen, W.-E. Liu, H. Ke, S.-H. Wang, W. Jiang, *J. Am. Chem. Soc.* **2017**, *139*, 8436–8439.

[17]   a) D. Chu, W. Gong, H. Jiang, X. Tang, Y. Cui, Y. Liu, *CCS Chemistry* **2022**, *4*, 1180–1189; b) Q.-P. Hu, H. Zhou, T.-Y. Huang, Y.-F. Ao, D.-X. Wang, Q.-Q. Wang, *J. Am. Chem. Soc.* **2022**, *144*, 6180–6184; c) Y. Ding, C. Shen, F. Gan, J. Wang, G. Zhang, L. Li, M. Shu, B. Zhu, J. Crassous, H. Qiu, *Chin. Chem. Lett.* **2021**, *32*, 3988–3992; d) L. Cheng, K. Liu, Y. J. Duan, H. H. Duan, Y. W. Li, M. Gao, L. P. Cao, *CCS Chemistry* **2021**, *3*, 2749–2763; e) X. H. Tang, H. Jiang, Y. B. Si, N. Rampal, W. Gong, C. Cheng, X. Kang, D. Fairen-Jimenez, Y. Cui, Y. Liu, *Chem* **2021**, *7*, 2771–2786; f) M. Yamamura, T. Saito, T. Hasegawa, E. Nishibori, T. Nabeshima, *Chem. Commun.* **2021**, *57*, 8754–8757; g) B. Li, W. Zhang, S. Lu, B. Zheng, D. Zhang, A. Li, X. Li, X.-J. Yang, B. Wu, *J. Am. Chem. Soc.* **2020**, *142*, 21160-21168.

[18]   a) I. Osadchuk, H. E. Luts, K. Norvaisa, V. Borovkov, M. O. Senge, *Chem. Eur. J.* **2023**, *29*, e202301408; b) I. Osadchuk, N. Konrad, K.-N. Truong, K. Rissanen, E. Clot, R. Aav, D. Kananovich, V. Borovkov, *Symmetry* **2021**, *13*, 275; c) A. Dhamija, P. Mondal, B. Saha, S. P. Rath, *Dalton Trans.* **2020**, *49*, 10679–10700; d) L. Ustrnul, S. Kaabel, T. Burankova, J. Martõnova, J. Adamson, N. Konrad, P. Burk, V. Borovkov, R. Aav, *Chem. Commun.* **2019**, *55*,

14434–14437; e) V. V. Borovkov, J. M. Lintuluoto, Y. Inoue, **2001**, *123*, 2979–2989.

[19]   a) A. Benchohra, S. Séjourné, A. Labrunie, L. Miller, E. Charbonneau, V. Carré, F. Aubriet, M. Allain, M. Sallé, S. Goeb, *Inorganics* **2022**, *10*, 103; b) S. Séjourné, A. Labrunie, C. Dalinot, A. Benchohra, V. Carré, F. Aubriet, M. Allain, M. Sallé, S. Goeb, *Inorganics* **2020**, *8*, 1.

[20]   a) R. Zhu, J. Ding, L. Jin, H. Pang, *Coord. Chem. Rev.* **2019**, *389*, 119–140; b) M. Frank, M. D. Johnstone, G. H. Clever, *Chem. Eur. J.* **2016**, *22*, 14104–14125; c) G. Gil-Ramírez, D. A. Leigh, A. J. Stephens, *Angew. Chem. Int. Ed.* **2015**, *54*, 6110–6150.

[21]   a) B. P. Benke, T. Kirschbaum, J. Graf, J. H. Gross, M. Mastalerz, *Nat. Chem.* **2023**, *15*, 413–423; b) P. Wagner, F. Rominger, J. H. Gross, M. Mastalerz, *Angew. Chem. Int. Ed.* **2023**, *62*, e202217251; c) Y. Wu, Q. H. Guo, Y. Qiu, J. A. Weber, R. M. Young, L. Bancroft, Y. Jiao, H. Chen, B. Song, W. Liu, Y. Feng, X. Zhao, X. Li, L. Zhang, X. Y. Chen, H. Li, M. R. Wasielewski, J. F. Stoddart, *Proc Natl Acad Sci USA* **2022**, *119*, e2118573119; d) Y.-Y. Zhang, F.-Y. Qiu, H.-T. Shi, W. Yu, *Chem. Commun.* **2021**, *57*, 3010–3013; e) A. Kumar, P. S. Mukherjee, *Chem. Eur. J.* **2020**, *26*, 4842–4849; f) T. K. Ronson, Y. Wang, K. Baldridge, J. S. Siegel, J. R. Nitschke, *J. Am. Chem. Soc.* **2020**, *142*, 10267–10272; g) Y.-W. Zhang, S. Bai, Y.-Y. Wang, Y.-F. Han, *J. Am. Chem. Soc.* **2020**, *142*, 13614–13621; h) W.-Z. Qiao, T.-Q. Song, P. Cheng, B. Zhao, *Angew. Chem. Int. Ed.* **2019**, *58*, 13302–13307; i) T. R. Schulte, J. J. Holstein, G. H. Clever, *Angew. Chem. Int. Ed.* **2019**, *58*, 5562–5566; j) W. M. Bloch, J. J. Holstein, B. Dittrich, W. Hiller, G. H. Clever, *Angew. Chem. Int. Ed.* **2018**, *57*, 5534–5538; k) R. Zhu, I. Regeni, J. J. Holstein, B. Dittrich, M. Simon, S. Prévost, M. Gradzielski, G. H. Clever, *Angew. Chem. Int. Ed.* **2018**, *57*, 13652–13656; l) Q. Wang, C. Yu, C. Zhang, H. Long, S. Azarnoush, Y. Jin, W. Zhang, *Chem. Sci.* **2016**, *7*, 3370–3376; m) Q. Wang, C. Yu, H. Long, Y. Du, Y. Jin, W. Zhang, *Angew. Chem. Int. Ed.* **2015**, *54*, 7550–7554; n) A. Mishra, A. Dubey, J. W. Min, H. Kim, P. J. Stang, K.-W. Chi, *Chem. Commun.* **2014**, 7542–7544; o) D. Samanta, P. S. Mukherjee, *J. Am. Chem. Soc.* **2014**, *136*, 17006–17009; p) T. Hasell, X. Wu, J. T. Jones, J. Bacsa, A. Steiner, T. Mitra, A. Trewin, D. J. Adams, A. I. Cooper, *Nat. Chem.* **2010**, *2*, 750-755; q) M. Fujita, N. Fujita, K. Ogura, K. Yamaguchi, *Nature* **1999**, *400*, 52-55.

[22]   N. P. E. Barry, J. Furrer, B. Therrien, *Helv. Chim. Acta* **2010**, *93*, 1313–1328.

[23]   a) O. de Frutos, T. Granier, B. Gomez-Lor, J. Jimenez-Barbero, A. Monge, E. Gutierrez-Puebla, A. M. Echavarren, *Chem. Eur. J.* **2002**, *8*, 2879–2890; b) A. L. Kanibolotsky, R. Berridge, P. J. Skabara, I. F. Perepichka, D. D. C. Bradley, M. Koeberg, *J. Am. Chem. Soc.* **2004**, *126*, 13695–13702.

[24]   X. Wang, Y. Wang, H. Yang, H. Fang, R. Chen, Y. Sun, N. Zheng, K. Tan, X. Lu, Z. Tian, X. Cao, *Nat. Commun.* **2016**, *7*, 12469.

[25]   Deposition numbers 2262273 (for L), 2262274 (for Ru6L2), 2262275 (for (Ru6L2)2) and 2262276 (for PDI-1@Ru6Lc2) contain the supplementary crystallographic data for this paper. These data are provided free of charge by the joint Cambridge Crystallographic Data Centre and Fachinformationszentrum Karlsruhe Access Structures service.

[26]   One should note that subscripts (1 and 2) which are used to differentiate between the diastereotopic protons of a given stereoisomer appear in full NMR spectra in SI file.

[27]   L. Avram, Y. Cohen, *Chem. Soc. Rev.* **2015**, *44*, 586–602.

[28]   J. C. Bailar, *J. Inorg. Nucl. Chem.* **1958**, *8*, 165–175.

[29]   P. Govindaswamy, D. Linder, J. Lacour, G. Süss-Fink, B. Therrien, *Chem. Commun.* **2006**, 4691–4693.

[30]   a) S.-L. Huang, T. S. A. Hor, G.-X. Jin, *Coord. Chem. Rev.* **2017**, *333*, 1–26; b) W. X. Gao, H. J. Feng, B. B. Guo, Y. Lu, G. X. Jin, *Chem. Rev.* **2020**, *120*, 6288–6325.

[31]   Acetonitrile-d3 has been chosen for complexation studies as the resulting spectra exhibit higher resolution than those obtained in methanol-d4.

[32]   M. Dekhtiarenko, S. Pascal, M. Elhabiri, V. Mazan, D. Canevet, M. Allain, V. Carré, F. Aubriet, Z. Voitenko, M. Sallé, O. Siri, S. Goeb, *Chem. Eur. J.* **2021**, *27*, 15922–15927.

[33]   J. Freudenreich, J. Furrer, G. Süss-Fink, B. Therrien, **2011**, *30*, 942–951.

WILEY-VCH

RESEARCH ARTICLE

Entry for the Table of Contents
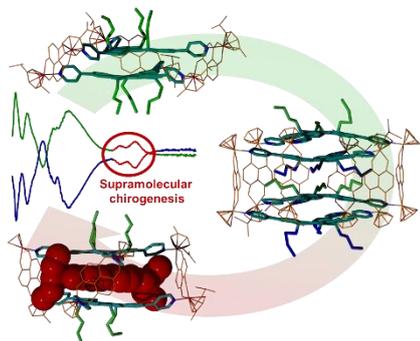
A chiral self-assembled cage constructed from the truxene framework dimerizes in solution thanks to favourable geometric and electronic parameters. The interlocked dimer can be dissociated upon forming a 1:1 host-guest complex in presence of a guest. The chiral cavity induces chirality in the achiral guest molecule as characterized by circular dichroism measurements.